Acta Biomaterialia 114 (2020) 170–182

Contents lists available at ScienceDirect

Acta Biomaterialia

journal homepage: www.elsevier.com/locate/actbio

Full length article

Engineering 3D functional tissue constructs using self-assembling cell-laden microniches

Dan Xing[a,b,1], Wei Liu[c,1], Jiao Jiao Li[d], Longwei Liu[e], Anqi Guo[c], Bin Wang[f], Hongsheng Yu[c], Yu Zhao[a,b], Yuling Chen[g], Zhifeng You[c], Cheng Lyu[c], Wenjing Li[c], Aifeng Liu[h], Yanan Du[c,**], Jianhao Lin[a,b,*]

[a] Arthritis Clinic & Research Center, Peking University People's Hospital, Peking University, Beijing 100044, China
[b] Arthritis Institute, Peking University, Beijing 100044, China
[c] Department of Biomedical Engineering, School of Medicine, Tsinghua-Peking Center for Life Sciences, MOE Key Laboratory of Bioorganic Phosphorus Chemistry and Chemical Biology, Tsinghua University, Beijing 100084, China
[d] School of Biomedical Engineering, Faculty of Engineering and IT, University of Technology Sydney (UTS), Ultimo, NSW 2007, Australia
[e] Institute of Engineering in Medicine, University of California, San Diego, La Jolla, CA 92093, USA
[f] Department of Sports Medicine and Adult Reconstruction Surgery, Nanjing Drum Tower Hospital, the Affiliated Hospital of Nanjing University Medical School, Nanjing 210009, China
[g] Tsinghua University-Peking University Joint Center for Life Sciences, Beijing 100084, China
[h] Department of Orthopedics, First Teaching Hospital of Tianjin University of Traditional Chinese Medicine, Tianjin 300193, China

ARTICLE INFO

Article history:
Received 15 April 2020
Revised 29 July 2020
Accepted 31 July 2020
Available online 6 August 2020

Keywords:
Functional tissue construct
Self-assembly
Hydrogel
Extracellular matrix
Cartilage repair

ABSTRACT

Tissue engineering using traditional size fixed scaffolds and injectable biomaterials are faced with many limitations due to the difficulties of producing macroscopic functional tissues. In this study, 3D functional tissue constructs were developed by inducing self-assembly of microniches, which were cell-laden gelatin microcryogels. During self-assembly, the accumulation of extracellular matrix (ECM) components was found to strengthen cell-cell and cell-ECM interactions, leading to the construction of a 'native' microenvironment that better preserved cell viability and functions. MSCs grown in self-assembled constructs showed increased maintenance of stemness, reduced senescence and improved paracrine activity compared with cells grown in individual microniches without self-assembly. As an example of applying the self-assembled constructs in tissue regeneration, the constructs were used to induce *in vivo* articular cartilage repair and successfully regenerated hyaline-like cartilage tissue in the absence of other extrinsic factors. This unique approach of developing self-assembled 3D functional constructs holds great promise for the generation of tissue engineered organoids and repair of challenging tissue defects.

Statement of Significance

We developed 3D functional tissue constructs using a unique gelatin-based microscopic hydrogel (microcryogels). Mesenchymal stem cells (MSCs) were loaded into gelatin microcryogels to form microscopic cell-laden units (microniches), which were induced to undergo self-assembly using a specially designed 3D printed frame. Extracellular matrix accumulation among the microniches resulted in self-assembled macroscopic constructs with superior ability to maintain the phenotypic characteristics and stemness of MSCs, together with the suppression of senescence and enhanced paracrine function. As an example of application in tissue regeneration, the self-assembled constructs were shown to successfully repair articular cartilage defects without any other supplements. This unique strategy for developing 3D functional tissue constructs allows the optimisation of stem cell functions and construction of biomimetic tissue organoids.

© 2020 Acta Materialia Inc. Published by Elsevier Ltd. All rights reserved.

* Corresponding author at: Arthritis Clinic & Research Center, Peking University People's Hospital, Peking University, Beijing 100044, China
** Corresponding author at: Department of Biomedical Engineering, School of Medicine, Tsinghua-Peking Center for Life Sciences, MOE Key Laboratory of Bioorganic Phosphorus Chemistry and Chemical Biology, Tsinghua University, Beijing 100084, China
E-mail addresses: duyanan@tsinghua.edu.cn (Y. Du), linjianhao@pkuph.edu.cn (J. Lin).
[1] The first two authors contributed equally to this work.

https://doi.org/10.1016/j.actbio.2020.07.058
1742-7061/© 2020 Acta Materialia Inc. Published by Elsevier Ltd. All rights reserved.

1. Introduction

Various types of stem cells are attractive cell sources for tissue engineering due to their capacity for self-renewal and ability to undergo pluripotent or multipotent differentiation. Certain types of stem cells, such as mesenchymal stem cells (MSCs), can also secrete beneficial factors that promote healing in surrounding tissues through paracrine mechanisms. The regulation of stem cell activity and fate using biomaterial scaffolds is a critical component of tissue engineering approaches to repair or regenerate diseased and damaged tissues [1,2]. When grown within a scaffold, stem cells perceive the scaffold as their microenvironment and respond accordingly by changing their behaviour. Methods that enable precise control over scaffold properties and an increased understanding of cell-material interactions are therefore crucial for establishing clinically useful stem cell-based tissue engineering technologies.

Hydrogels are often used for tissue engineering due to their superior tunability compared to other forms of scaffolds, allowing precise control over important scaffold properties such as stiffness, density, composition, permeability, and degradability, all of which have profound effects on cell activity and fate [3–5]. Various well-defined synthetic hydrogels have emerged as promising scaffolds for cell therapy. For instance, recent developments include fine-tunable hydrogels for cell delivery that can guide the activity and fate of MSCs by incorporating integrin-binding small molecules [6] or bioactive peptides [7]. Although hydrogels are a promising tool for studying cell-material interactions or as a cell carrier to promote tissue repair, their applications in tissue engineering face some common challenges. First, the requirement for cross-linking may limit the *in vivo* applications of both natural and synthetic hydrogels. For instance, UV cross-linking may be harmful to cells depending on the wavelength used, where UV light of 254 nm can cause much higher damage to cellular physiology than longer wavelengths of around 350 nm [8]. Physical cross-linking can result in hydrogels that are easily disrupted by mechanical loads [9], and chemical cross-linking may be associated with some degree of toxicity to the encapsulated cells, due to the use of chemical agents with biologically incompatible features [10,11].Although hydrogels can be formed *in situ* through enzyme-catalysed mild cross-linking reactions, these cell-friendly methods are mostly substrate-specific and remain underexplored. Second, many tissue engineering applications benefit from the ability to maintain the cells used in a native environment that minimises cell senescence and preserves their functional phenotype. However, this is a challenge for most conventional hydrogel systems which often increase cell senescence with prolonged culture within the hydrogel [12], and/or change the ability of stem cells to maintain their 'stemness' [13] or secrete paracrine factors [14].

To overcome the limitations of conventional hydrogel systems, recent studies have investigated the development of self-crosslinking hydrogels. These hydrogels have been made from blends of various natural and synthetic materials including alginate, collagen, hyaluronic acid, gelatin and polyethylene glycol, and tested using different cell types such as MSCs [10] and chondrocytes for cartilage [15] and meniscus repair [16]. However, the methods used to induce self-crosslinking are specific to these hydrogel systems and not broadly applicable to other hydrogel formulations. In addition, these self-crosslinking hydrogels may cause damage to the encapsulated cells during the gelation process, and/or limit cell activity after gelation by restricting extracellular matrix (ECM) deposition and cell-cell interactions.

As an alternative or supplement to hydrogel systems, porous microspheres can be used with some attractive advantages, including good biocompatibility, large specific surface area and ease of interaction with drug molecules [17]. These microspheres have interconnected external and internal pores that provide immense surface area for cell attachment and growth, while facilitating efficient transport of nutrients, oxygen and waste products. Combining the advantages of hydrogels and microspheres, we previously developed injectable microcryogels which were microscale macroporous cryogels. Instead of only increasing the surface area, as for traditional porous microspheres, our microcryogels provide a 3D microenvironment that enables automatic and homogeneous loading of cells, matrices, and/or bioactive factors to construct tailored cellular niches. Different cell types were loaded into these microcryogels to form 3D cell-laden 'microniches' that could be used for site-directed and augmented cell therapy, which we have applied in various experimental models including limb ischaemia, disc degeneration, wound healing and liver cirrhosis [18–23]. We further confirmed that the physical properties of these microniches, namely pore size and stiffness, can be controlled to modulate tissue regeneration [24,25].Compared to conventional hydrogel systems, these microniches can shield cells from mechanical insult and provide a porous microenvironment that better maintains cell viability and functionality. The microniches have shown promising therapeutic effects in *ex vivo* and *in vivo* models of various pathological conditions. However, the *in vivo* applications so far have involved injecting the microniches directly into small defects (e.g. mouse skin wound [23]) or tissues that do not require the injected material to conform to a specific shape (e.g. canine intervertebral disc [20]). To facilitate broader and more practical applications in tissue engineering, such as to study cell behaviour in functional tissue organoids replicating the structure of native tissues, or to repair tissue defects of clinically-relevant sizes and defined shapes (e.g. knee articular cartilage), macroscale tissue constructs with customisable shapes and sizes need to be developed. For instance, injectable MSC-laden microgels could be used as building blocks to create an assembled construct through a chemical cross-linking process [26], which improved the chondrogenic phenotype of encapsulated chondrocytes [27]. 3D constructs assembled using cell-laden microscopic hydrogels are therefore an attractive method for applications in tissue regeneration.

In this study, we developed macroscale tissue constructs by inducing self-assembly of microniches using a 3D-printed permeable frame. The shape and size of the construct can be customised by altering the 3D printing parameters for producing the frame. MSCs were loaded onto microcryogels to form the microniches, which were placed inside the frame and cultured for several days to induce self-assembly into functional tissue constructs. MSCs were chosen as the source cells in this study due to their popular use in tissue engineering and easy accessibility, and more importantly their 'environmental responsiveness' [28] that is highly relevant for evaluating cell behaviour within the self-assembled tissue constructs. We found that MSCs within self-assembled microniche constructs maintained their stemness and paracrine functions to a greater extent than cells within non-self-assembled microniches. Mechanistic studies indicated that self-assembly was induced by connection of microniches through ECM accumulation secreted by MSCs. We also investigated the treatment effects of using these self-assembled constructs in tissue repair, using a rabbit articular cartilage defect model as an example. The self-assembling hydrogel-based tissue constructs developed in this study addressed several major challenges of traditional hydrogel systems, such as cytotoxicity due to cross-linking and inability to maintain functional phenotype of the encapsulated cells. This strategy may have new applications in establishing functional *in vitro* models of tissue development and pathology, as well as repairing macroscopic and irregular tissue defects that require integration of the tissue engineered construct with native tissues.

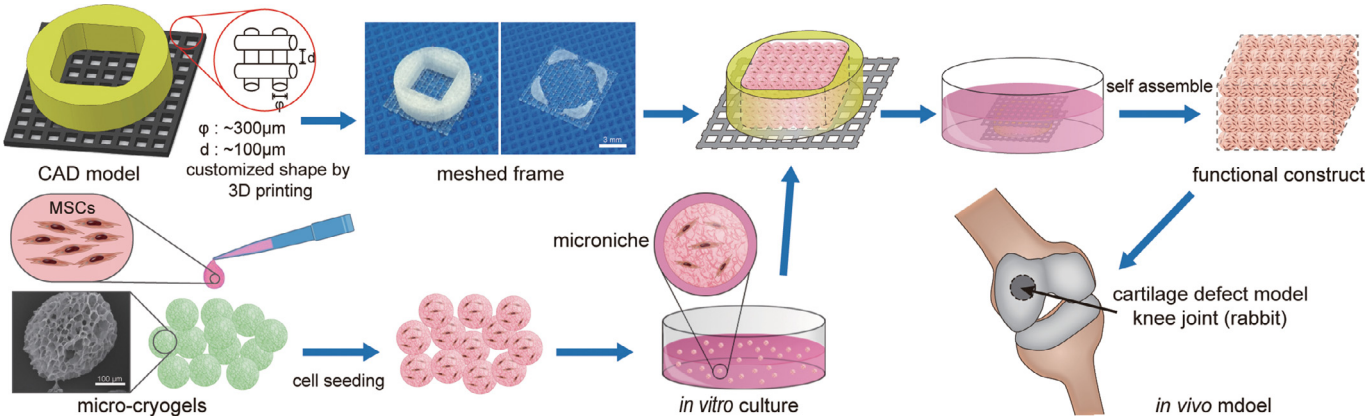


Fig. 1. Schematic illustration of the overall study design.Microniches were made from MSC-laden microcryogels. These were placed within 3D-printed meshed frames to induce self-assembly into functional tissue constructs. The constructs were evaluated for their effects on cell behaviour compared to non-self-assembled microniches *in vitro*, as well as tissue repair *in vivo* using an articular cartilage defect model as an example.

2. Materials and methods

2.1. Experimental design

An overview of the study design is shown in Fig. 1. The customised meshed frame was made by 3D printing using PLA (eSUN Co., Ltd). Through a series of processes involving gelatin microcryogel fabrication, cell seeding and culture, MSC-laden microniches (3D-free group) were made and loaded into the meshed frame. Functional constructs (3D-construct group) were formed by self-assembly of the MSC-laden microniches over several days of culture. The groups were compared through *in vitro* analyses and *in vivo* implantation into articular cartilage defects in the rabbit trochlear groove. MSCs cultured in monolayer (2D group) were used as a control for specific *in vitro* experiments.

2.2. Preparation of MSC-laden microniches

2.2.1. Microcryogel fabrication

Gelatin microcryogels were developed based on previously published methods [18,19]. Briefly, PMMA microstencil array chips, each containing 600 circular micro-wells with diameter of 200 μm were made using a laser fabrication system (Rayjet) and treated with a plasma cleaner (Mycro Technologies) to increase hydrophilicity. A gelatin precursor solution (4% w/v gelatin) was made by dissolving the gelatin at 50°C in a water bath, followed by chilling on ice for 5 min and adding 70 μL of 0.5% glutaraldehyde solution with mild stirring. This precursor solution was pipetted in a 250 μL aliquot onto the upper surface of each PMMA chip and manually scraped across the chip surface to ensure an even distribution. The filled chip then underwent cryogelation for 16 h at -20°C, followed by lyophilisation for 30 min (Boyikang). The gelatin microcryogels were harvested using a PMMA ejector pin array fabricated with a desktop 3D milling machine (MDX-40A; Roland DG), washed with0.1 M $NaBH_4$ to neutralise any unreacted aldehyde, and then washed thoroughly with distilled water. Microcryogels were placed into a dish in an even monolayer, lyophilised and vacuum-packaged until use in downstream experiments.

2.2.2. Cell culture and seeding

Prior to cell seeding, lyophilised microcryogels were sterilised by ethylene oxide (AN74j/Anprolene; Anderson Sterilisation). Human umbilical cord MSCs (EUBIO Technologies) was cultured in MSC growth medium (BioWit Technologies) as previously described [20]. MSCs were seeded onto 20 mg microcryogels in a 40mm diameter cell culture dish through a 200 μL cell suspension (2.5 × 10^6cells/mL), which immediately hydrated and was absorbed into the microcryogels. The seeded microcryogels were incubated at 37°C in a humidified chamber for 2 h to allow cell adhesion [21], following which culture medium was added.

2.3. Preparation of self-assembled microniche constructs

2.3.1. 3D printing of meshed frames

Meshed frames with 7 mm (length) × 7 mm (width) × 4 mm (height) inner dimensions were designed using AUTOCAD software (Autodesk Inc) and made by PLA using a 3D printer (AOD printer Inc) (Fig. S1a). The mesh spacing was less than 100 μm to prevent overflow of microniches. The meshed frames were sterilised by soaking in 80% (v/v) ethanol overnight, rinsed three times with PBS and irradiated with UV prior to use.

2.3.2. Loading MSC-laden microniches in meshed frames to induce self-assembly

MSC-laden microniches were cultured at 37°C in a humidified chamber for 3 days prior to loading in the meshed frames. All the microniches in one 40 mm diameter cell culture dish were pipetted into each meshed frame, which was then cultured in MSC growth medium for 3, 7 and 14 days in a cell culture dish.

2.4. Characterisation of self-assembled microniche constructs

2.4.1. Morphological observation of self-assembled constructs

Self-assembled constructs were completely removed from the meshed frames at 3, 7 and 14 days after culture. For scanning electron microscopy (SEM) (FEI Quanta 200), samples were fixed in 10% neutral buffered formalin, dehydrated using graded ethanol, subjected to critical point drying, and sputtered with gold for 90 s. SEM imaging was performed to observe the morphology of constructs.

2.4.2. Cell viability within self-assembled constructs

Numbers of viable MSCs within the self-assembled constructs was determined using a CellTiter-Blue® cell viability assay. A standard curve was first constructed to determine the linear relationship between cell number and fluorescence intensity. Cell numbers were assessed at 0, 3, 7 and 14 days, by calculating the number of cells per construct using the standard curve. Relative cell proliferation was calculated from the numbers of viable MSCs at each time point. The viability of cells within the constructs was additionally visualised using live/dead staining (Life Technologies).

2.4.3. Cell apoptosis assay

MSCs were digested from self-assembled constructs by using 0.1% collagenase I for 30 min at 37°C.PBS was added to stop the digestion, after which the samples were centrifuged at 1,000 rpm for 5 min. A 100 µL volume of MSC suspension (1×10^5cells/mL) was used for testing. Apoptotic cells were evaluated using an annexin V/propidium iodide (PI) double staining apoptosis detection kit (Beyotime Technologies). The MSCs were stained according to the manufacturer's instructions and analysed by flow cytometry (BD LSRFortessa SORP, USA).

2.4.4. Macroscopic and microscopic mechanical testing of self-assembled constructs

For macroscopic mechanical testing, the self-assembled constructs were immersed in PBS and tested under unconfined compression using an ElectroForce 3200 mechanical tester (BOSE, USA). The constructs were compressed at 0.05mm/s for up to 4 mm, and the compressive load was recorded. Young's modulus was calculated from the linear slope of the stress–strain curve.

For microscopic mechanical testing, the self-assembled constructs were collected, frozen in liquid nitrogen for 1h, dried for 30h, and vacuum-packaged until use. The constructs were grinded into fragments and placed on a glass slide for testing. Micromechanical compression testing was conducted by atomic force microscopy (AFM) using the AFM module Cellhesion® 200 (JPK Instruments), where samples were mounted on an inverted fluorescence microscope (Zeiss Observer A1 stand). The silicon tipless cantilever (ARROW-TL1-50, NANOWORLD) used to indent the samples had a nominal spring constant of 0.03 N/m, and was attached with a silicon microsphere (6 µm diameter) on the cutting edge. For each sample, at least 25 different indentation locations were tested with up to ~2nN force at 5µm/s displacement rate. The effective indentation modulus was obtained by fitting the load-displacement curve to the Hertz model (the Poisson's ratio was set to be 0.5).

2.5. Functional assessment of self-assembled constructs

2.5.1. Trilineage differentiation of MSCs

Trilineage differentiation ability of MSCs was assessed by culturing the cells with StemPro® (Gibco, Life Technologies) differentiation media to induce osteogenesis, chondrogenesis and adipogenesis. Osteogenesis was assessed at 14 days by staining the cells for alkaline phosphatase with the BCIP/NBT Kit (Sigma-Aldrich) according to the manufacturer's instructions. Chondrogenesis was assessed at 14 days by staining for sulfated proteoglycan deposits with Alcian-Blue Staining Solution (Sigma-Aldrich). Adipogenesis was assessed at 21 days by staining for lipid accumulation using the Oil Red O Kit (Sigma-Aldrich).

2.5.2. Flow cytometry for phenotypic characterisation of MSCs

MSCs digested from monolayer or self-assembled constructs were stained with antibodies against MSC markers (CD34, CD44, CD73, CD90 and CD105). Unstained MSCs were used as negative controls. Cells were analysed by flow cytometry (BD LSRFortessa SORP). The analysis was conducted by pooling 3 constructs into one sample.

2.5.3. RNA isolation and quantitative RT-PCR (qRT-PCR)

RNA was isolated from MSCs using the TRIzol reagent (Invitrogen) according to the manufacturer's instructions. For each sample, 1 µg of RNA was reversely transcribed using the PrimeScript 1st strand cDNA Synthesis Kit (Takara Bio USA). qRT-PCR was performed using the SYBR Premix Ex Taq (Takara), together with 2.5 ng of cDNA and forward and reverse primers, and quantified using the CFX96 Real-Time System (Bio-Rad). Expression levels of all genes were normalised against the reference gene GAPDH using the comparative Ct ($2^{-\Delta\Delta CT}$) method. All primers used are listed in Table S1.

2.5.4. Western blot

Total protein from MSCs was extracted using RIPA lysis buffer (Beyotime) supplemented with protease inhibitors PMSF (Beyotime) according to the manufacturer's instructions. Proteins were separated on 10–12% SDS/PAGE gels and transferred onto a PVDF membrane (Millipore). The proteins were detected by secondary antibodies and Super-Signal West Pico Chemiluminescent Substrate (Thermo Fisher) using the ChemiDoc XRS+ System with Image Lab software(Bio-Rad). All antibodies used are listed in Table S2.

2.5.5. β-Gal assay

The SA-β-Gal activity of MSCs was measured using a senescence β-galactosidase staining kit (Beyotime). Briefly, MSCs were digested from monolayer or self-assembled constructs, seeded in a six-well plate (1×10^6 cells/well) and cultured for 12 h until MSCs adhered to the plate.SA-β-Gal staining was conducted according to the manufacturer's instructions. The MSCs were observed using an Olympus BX51 microscope, and senescent cells were counted.

2.5.6. Secretome analysis

Monolayer MSCs or self-assembled constructs with a similar number of cells were washed twice in PBS and cultured under starvation in non-supplemented α-MEM for 24 h. The culture supernatants were collected and analysed for 105 secreted proteins using the Proteome Profiler Human XL Cytokine Array Kit (R&D Systems, catalogue numberARY022) according to the manufacturer's instructions. Briefly, the stamped identification number of each membrane was cut off and replaced with an individual mark using a pencil. Each membrane was blocked, washed and incubated overnight at 4°C on a rocking platform with 1.5 mL of culture supernatant diluted at a 1:3 ratio using the supplied array buffer. Membranes were washed and incubated with the detection antibody cocktail for 1 h at room temperature on a rocking platform. The membranes were imaged using the ChemiDoc XRS+ System with Image Lab software (Bio-Rad). Pixel density of the spots was measured using the HLImage++ software (Western Vision, USA). After correcting for background intensity and normalising to the membrane's positive control, expression levels of cytokines were detected by array analysis and drawn as a heat map. Pairs of reference spots in the three corners of each array were used as the membrane's positive control.

2.6. Mechanistic investigations of construct self-assembly

2.6.1. Quantitative proteomics assay

Protein extraction from self-assembled constructs was conducted at 0, 3, 7 and 14 days of culture according to our published methods [29,30].Total protein concentration was measured using the BCA Assay Kit (Thermo Fisher) according to the manufacturer's instructions. For each sample, 200 µg protein in 200 µL protein extraction buffer was reduced by 5 mM dithiothreitol (DTT) at room temperature for 1 h, and alkylated by 12.5 mM iodoacetamide (IAM) at 25°C for 1 h in the dark. The samples were diluted to 1.5 M urea in PBS and digested with trypsin at a 100:1 protein/trypsin ratio overnight at 37°C. Peptides were desalted using Sep-Pak C18 columns (Waters, USA) and labelled with Tandem Mass Tag (TMT) 6-plex labelling reagent (Thermo Fisher). LC-MS/MS analysis was performed according to published methods [29,30].The raw spectra data were searched against the NCBI protein database (ftp://ftp.ncbi.nlm.nih.gov/genomes/Sus_scrofa/protein/)on the SEQUEST search engine in the Proteome Discoverer software (Thermo Fisher).The ratio of each protein between samples was calculated

using the average proportion of peptide spectral matches (PSMs) belonging to the protein. All identified proteins were used for further analysis.

2.6.2. Bioinformatic analysis

We defined protein expression of self-assembled constructs at 3, 7 and 14 days as higher expression if the expression was above 1.5-fold higher compared to 0 days, and lower expression if the expression was below 0.6-fold change. Hierarchical clustering was performed for both the protein and sample and drawn as a clustering heat map by R software. Protein family classification for all detected proteins, the cellular component, and molecular function of DRPs were performed using Panther (www.pantherdb.org).In Gene Ontology (GO) enrichment process, the cellular components, biological process, molecular function and protein signalling pathway analyses were performed using DAVID 6.8 (https://david.ncifcrf.gov/).The Protein-Protein Interaction (PPI) network was constructed on STRING version 11.0 (https://string-db.org/), and the clustering interaction score filter of the PPI network was of confidence $\geq$ 0.4. Western blot was conducted to confirm the results of proteomics assay by pooling 3 constructs into one sample.

2.7. In vivo *experiment*

2.7.1. Rabbit femoral trochlear cartilage defect model

The *in vivo* experiment has been conducted according to protocols approved by the Institutional Animal Care and Use Committee at Peking University Peoples' Hospital. Twenty-four healthy adult male New Zealand white rabbits (weight 3.0-3.5 kg) were used to create the femoral trochlear cartilage defect model. Animals were anaesthetised with 3% sodium pentobarbital, following which a cartilage defect (3 mm diameter $\times$ 4 mm depth) was created with a sterile biopsy punch in the centre of the trochlear groove of the bilateral hind limbs. Rabbits were randomly divided into three groups according to the type of implant inserted into the cartilage defect: 3D-constructs group (self-assembled constructs of MSC-laden microniches, secured in the defect by applying fibrin glue to the surface); microcyogels group (microcryogels without MSCs, secured in the defect using fibrin glue); and control group (fibrin glue used to fill the defect). Rabbits were sacrificed by excessive anaesthesia at 3 and 6 months after surgery.

2.7.2. Gross morphological evaluation

Gross morphological evaluation was performed for each knee to evaluate defect filling, implant integration to border zone, and macroscopic appearance using International Cartilage Repair Society (ICRS) scores [31]. The samples were blindly scored by two independent assessors.

2.7.3. Histological and immunohistochemical evaluation

Harvested samples were fixed for 3 days in 4% paraformaldehyde and subsequently decalcified in 10% (w/v) EDTA for 6–8 weeks. Following dehydration through graded ethanol, samples were embedded in paraffin and cut into 5 µm sections. The sections were stained using haematoxylin and eosin (H&E) for morphological evaluation, safranin-O for glycosaminoglycan content, Alcian blue for chondrocytes, and Masson's trichrome for collagen fibres. Sections were also immunohistochemically stained for collagen types I, II and X (Abcam). Histological scoring of tissue repair within the defect was blindly conducted by two independent assessors using the ICRS histological scoring system (Table S3) [31]. Slide scanner microscope Axio Scan.Z1 (Zeiss, Germany) and Pannoramic Scan (3DHISTECH, Hungary) were used for image capture at the 3 and 6 month time points, respectively.

2.8. Statistical analysis

All data were expressed as mean $\pm$ standard deviation. After testing for homogeneity of variances, one-way analysis of variance (ANOVA) followed by Tukey's post hoc multiple comparisons test were used to determine significant differences between groups. SPSS 11.0 was used to perform statistical analyses, and values of $p < 0.05$ were considered statistically significant. In flow cytometry, proteomics assay and secretome analysis, three constructs were pooled into one sample for further study.

3. Results

3.1. Characterisation and functional evaluation of MSCs in self-assembled constructs compared to non-self-assembled microniches and monolayer culture

3.1.1. Characterisation of MSC phenotype

MSCs in the 2D, 3D-free and 3D-construct groups were cultured for 7 days, after which they were digested and seeded in a six-well plate, and cultured for 12 h. These were then used to perform trilineage differentiation assays and staining for MSC-specific markers. MSCs in all groups showed trilineage differentiation ability, as demonstrated through specific histological stains for osteogenesis, chondrogenesis and adipogenesis (Fig. 2a). All groups also showed positive staining by flow cytometry for the MSC-specific surface markers CD44, CD73, CD90 and CD105, as well as negative staining for CD45 and CD34 (Fig. 2b). Therefore, MSCs grown in self-assembled constructs could maintain their phenotype to a similar extent as those grown in non-self-assembled microniches and in 2D monolayer.

3.1.2. Characterisation of MSC stemness and senescence

MSCs in the 2D, 3D-free and 3D-construct groups were harvested at 7 days and analysed by qRT-PCR. The stemness-related markers NANOG and OCT4 showed significantly upregulated expression in the 3D-construct group compared to the 2D and 3D-free groups, while SOX2 showed no significant differences (Fig. 2c). The senescence-related markers P16, P21 and P53 showed significantly downregulated expression in the 3D-construct group compared to the other groups (Fig. 2d). Western blot and corresponding quantitation showed that protein expression of P21 and P53 in the 3D-construct group was significantly lower than other groups (Fig. 2e and f). Furthermore, senescence-associated beta-galactosidase (SA-β-Gal) staining revealed that the 3D-construct group had the highest inhibition of MSC senescence (Fig. 2g) and significantly lower percentage of SA-β-Gal+ cells (Fig. 2h). These results collectively suggest that MSCs in self-assembled constructs maintain their stemness and suppress senescence to a greater extent than cells grown in non-self-assembled microniches and in 2D monolayer.

3.1.3. Activation of MSC paracrine functions

The paracrine function of MSCs in the 2D, 3D-free and 3D-construct groups was assessed through secretome analysis of culture supernatants following cell starvation. The resulting cytokine profile of groups was compared (cytokine array blots shown in Fig. 2i; quantitative expression of all cytokines presented in Table S4). A total of 13 cytokines were highly expressed in the 3D-construct group compared to the other two groups (Fig. 2j). Based on the common functions of these cytokines, they can be classified into four categories: recruitment factors (DKK-1, MCP1), proliferation (Chitinase 3-like 1, GDF-15, GRO-α), immunomodulatory (Complement Factor D, MIF, Osteopontin, Rentraxin-3, ST2,Cystatin C), and angiogenesis (Angiogenin, VEGF). MSCs cultured within the self-assembled constructs may therefore increase their paracrine

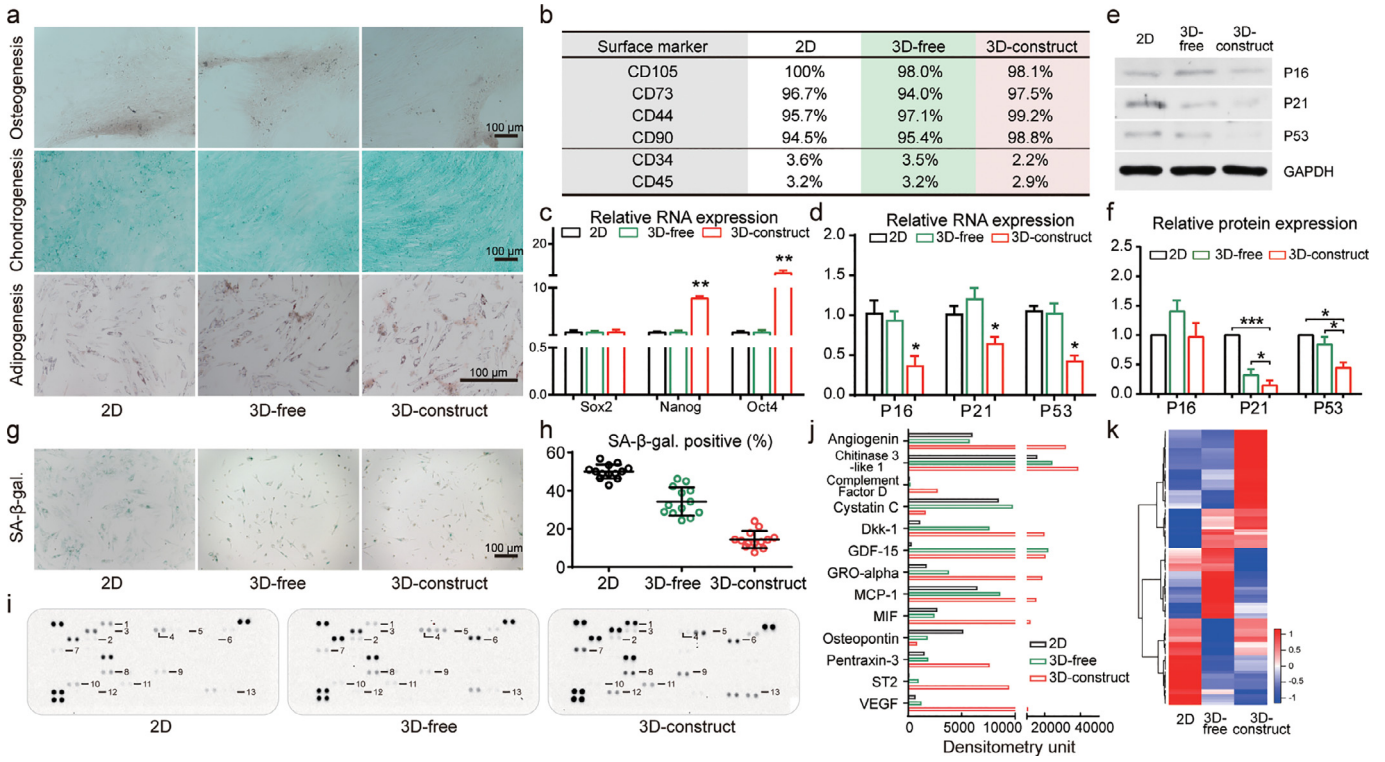


Fig. 2. Characterisation and functional evaluation of MSCs in self-assembled constructs compared to non-self-assembled microniches and monolayer culture. (A) Representative images of trilineage differentiation of MSCs in the 2D, 3D-free and 3D-construct groups ($n = 3$). (B) Flow cytometry analysis of surface biomarker expression of MSCs in the three groups ($n = 1$, correspondent to a pool of 3 constructs). (C) Relative gene expression of stemness-related markers (SOX2, NANOG, OCT4) in the three groups ($n = 3$). (D) Relative gene expression of senescence-related markers (P16, P21 and P53) in the three groups (n= 3). (E, F) Protein expression of senescence-related markers (P16, P21 and P53) in the three groups (n= 3). (G) Representative images of SA-β-Gal in MSCs and (H) percentage of SA-β-Gal+ cells, indicating that self-assembled constructs inhibited MSC senescence. Image analysis was performed in 13 images from 3 constructs ($n = 3$). (I) Representative images of cytokine array blots probed with culture supernatants of the three groups. Each blot represents immunoreactive staining against respective antibodies ($n = 3$). The blots marked with numbers indicate significantly up-regulated cytokines compared to the 2D group. (J) Relative expression levels of 13 up-regulated cytokines. (K) Heat map of all 105 incubated cytokines for the three groups.

function related to the functions of these cytokines. Comparison of the entire cytokine profile among groups is drawn as a heat map (Fig. 2k).

3.2. Characterisation of constructs and MSCs during self-assembly at different time points

3.2.1. Characterisation of constructs during self-assembly at different time points

A schematic of the timeline for characterisation of self-assembled constructs is presented in Fig. 3a. The MSC-laden microniches (diameter 200-300 <mu>m) were stacked into the 3D-printed frame, and the formation of a self-assembled construct was detected as early as day 3 of cell culture (Fig. S1b and MOVIE S1). The construct structure was maintained when released from the frame at 7 and 14 days (Fig. 3b). At 7 days, self-assembled constructs cultured in 3D-printed frames exhibited predefined shapes according to the inner geometry of the frame (Fig. S1c). SEM showed that at 3, 7 and 14 days, the self-assembled constructs consisted of microniches with gradually increasing ECM deposition which strengthened the connections between them (Fig. 3c).

Live/dead staining at the centre of self-assembled constructs showed that almost all MSCs were alive at 3 and 7 days (Fig. 3d), compared to MSCs cultured within a gelatin bulk scaffold made through traditional fabrication methods, where significant cell death had occurred by 7 days (Fig. S2). Prolonged static culture caused the number of dead cells to increase in the self-assembled constructs by 14 days (Fig. 3d and S1d). To further confirm cell death, Annexin V and PI double staining was used to label apoptotic and dying cells. The number of MSCs in self-assembled constructs that were undergoing apoptosis and cell death was relatively constant within 7 days of culture, but significantly increased at 14 days (Fig. e and f). Similarly, cell proliferation was greatly suppressed at 14 days, as shown by the numbers of viable MSCs found within the self-assembled constructs (Fig. 3g).

Fragments of self-assembled constructs were subjected to micro-mechanical testing using AFM. Local construct stiffness under compression increased with time in culture (Fig. 3h). In addition, mechanical testing conducted using whole self-assembled constructs showed a significant increase in Young's modulus under compression at 7 days (Fig. 3i). In both tests, the stiffness values were similar at 7 and 14 days, suggesting that 7 days were sufficient for significant construct maturation and ECM accumulation to provide satisfactory mechanical properties.

Analysis of MSC surface markers (Fig. 3j) and trilineage differentiation (Fig. 3k) in self-assembled constructs over 14 days showed no significant phenotypic changes at any of the time points. Collectively, the results suggested that MSC-laden microniches formed self-assembled constructs with optimal biological and mechanical properties when cultured for 7 days within the 3D-printed frames.

3.2.2. Functional analyses of MSCs in constructs during self-assembly at different time points

The stemness, senescence and paracrine functions of MSCs in constructs during self-assembly were evaluated. Stemness-related markers (SOX2, NANOG and OCT4) were significantly upregulated in MSCs at 7 days within the constructs compared to those at ear-

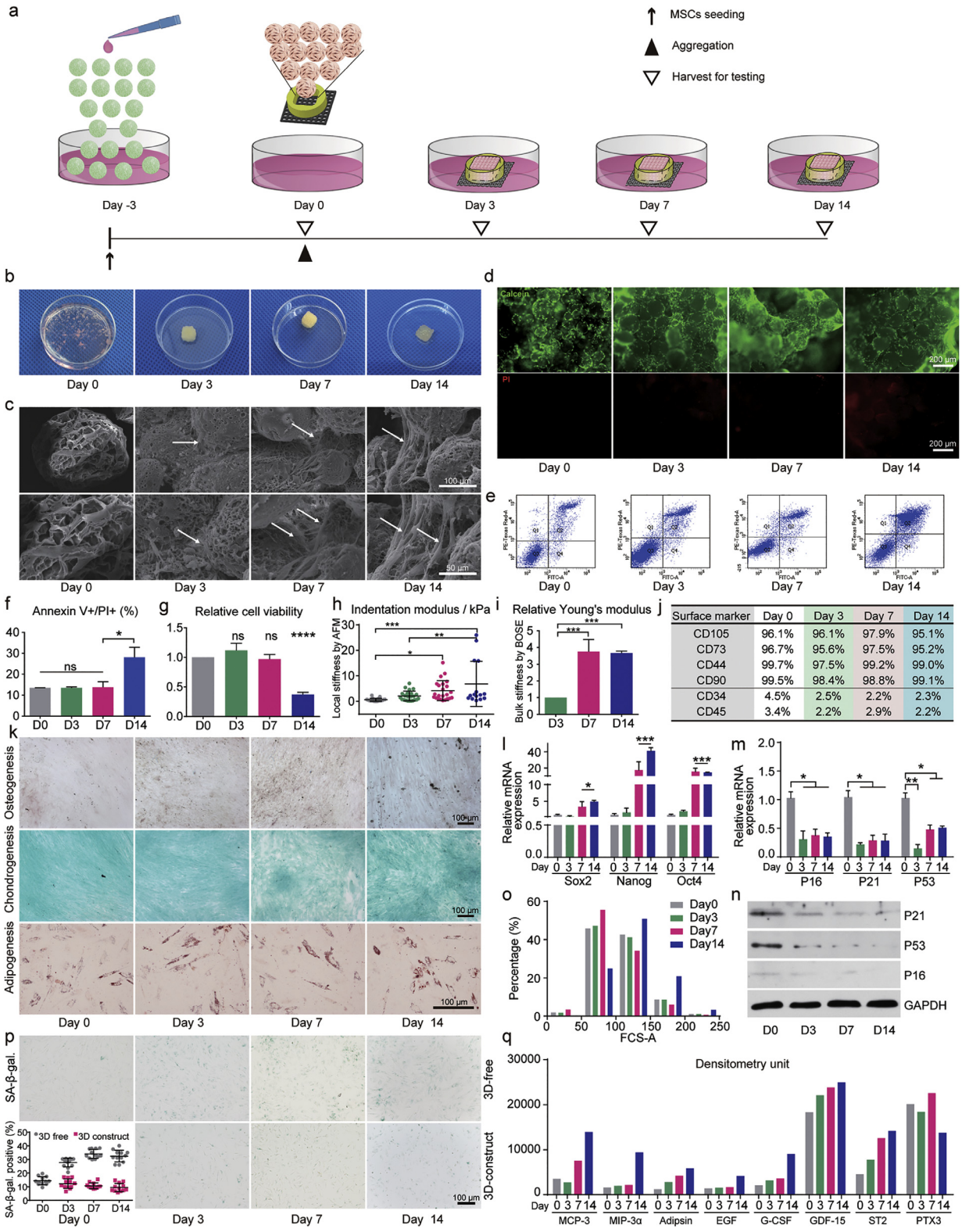


Fig. 3. Characterisation of constructs and MSCs during self-assembly at different time points. (A) Schematic illustration of the time points for characterising self-assembled constructs. (B) Morphology of constructs during self-assembly at 0, 3, 7 and 14 days; the MSC-laden microniches begin self-assembly at 3 days when cultured within the 3D-printed frame. (C) SEM images taken at different time points during construct self-assembly. Arrows indicate ECM deposition. (D) Fluorescence microscopy images of MSCs with live/dead staining in self-assembled constructs at different time points ($n = 3$). (E) Representative histograms showing the change in distribution of Annexin V and PI labelled cells in the total cell population during construct self-assembly, and (F) bar graph showing the percentage of apoptotic/dead cells ($n = 3$). (G) Relative cell viability of MSCs in constructs during self-assembly at different time points ($n = 3$). (H) Young's modulus of scaffold fragments under micro-mechanical compression by AFM ($n = 15$), and (I) Young's modulus of entire constructs under compression ($n = 3$), at different time points. (J) Flow cytometry analysis of surface biomarker expression ($n = 1$, correspondent to a pool of 3 constructs) and (K) representative images of trilineage differentiation of MSCs in constructs during self-assembly ($n = 3$). (L) Relative gene expression of stemness-related markers (SOX2, NANOG, OCT4) during self-assembly ($n = 3$). (M, N) Relative gene and protein expression of senescence-related markers (P16, P21 and P53) during self-assembly ($n = 3$). (O) Size distribution of MSCs in self-assembled constructs at different time points ($n = 3$). (P) Representative images of SA-β-Gal staining for MSCs in 3D-free and 3D-construct groups ($n = 12$). (Q) Relative expression levels of 8 upregulated cytokines secreted by MSCs in self-assembled constructs ($n = 3$).

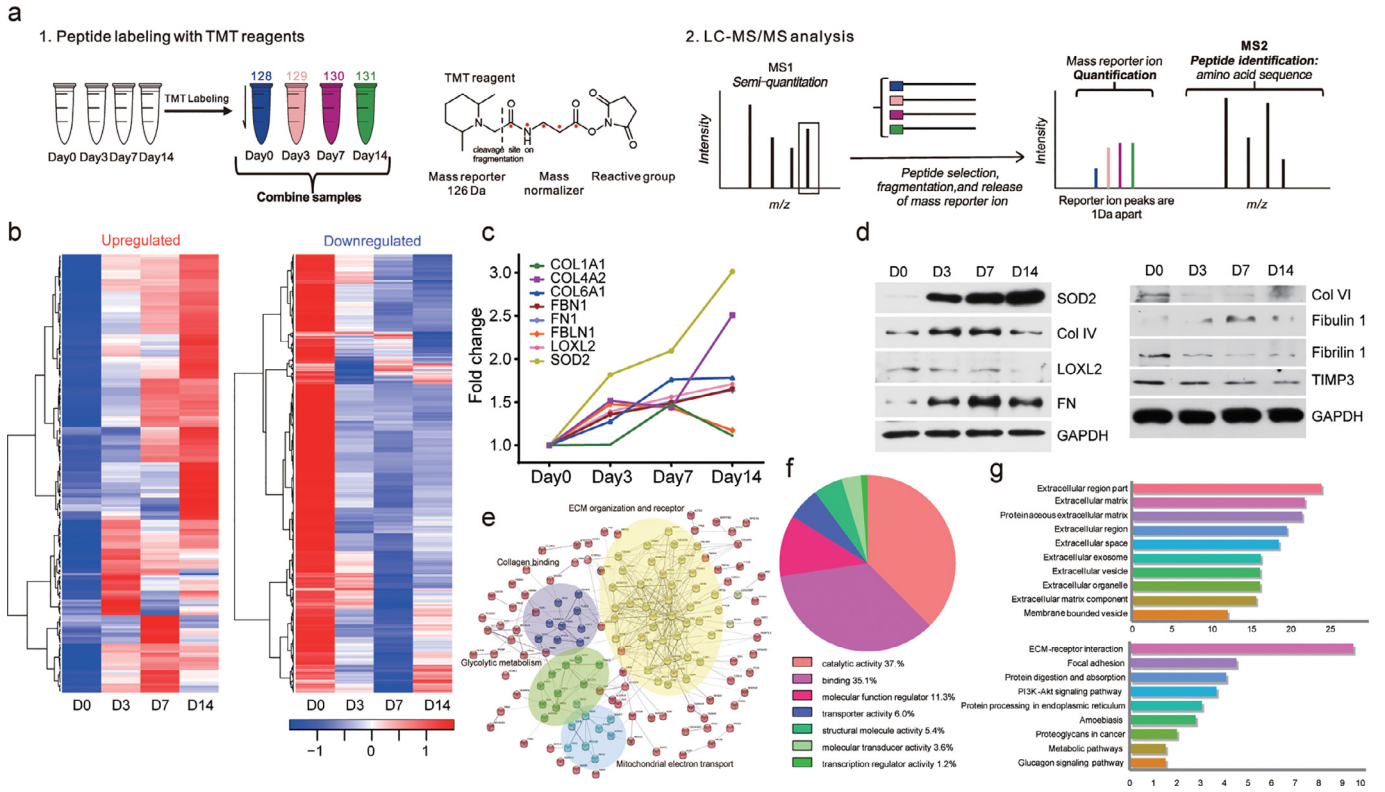


Fig. 4. Mechanism for self-assembly of microniches into functional constructs. (A) Schematic of TMT labelling for proteomic analysis. Four sample solutions labelled with aspecific TMT reagent (different colours) enable relative quantification after peptide separation and fragmentation. (B) Heat map of proteins indicating changes in relative expression during construct self-assembly. The heat maps show a total of 199 upregulated proteins compared with D0 (left), and1077 downregulated proteins compared with D0 (right). (C) Examples of proteins with significantly upregulated expression during construct self-assembly. (D) Western blot confirming the differences in relative protein expression as demonstrated in proteomic analysis (n= 1, correspondent to a pool of 3 constructs). (E) Protein-protein interaction analysis of all differentially upregulated proteins, which were classified into four clusters with STRING. (F) Classification of upregulated proteins during self-assembly by biological process through PANTHER. (G)Enrichment analysis of gene oncology (GO) terms for upregulated proteins during self-assembly, with the proteins assigned to two categories: cellular components (top panel) and signal pathway (bottom panel).

lier time points, and remained relatively stable at 14 days (Fig. 3l). On the other hand, senescence-related markers (P16, P21 and P53) were significantly downregulated as soon as the process of self-assembly had commenced at 3 days, and remained at similar levels thereafter (Fig. 3m). These trends were confirmed by protein expression of the same senescence-related markers (Fig. 3n). Cell size measured using flow cytometry can be used as an additional indicator of senescence, since smaller cell sizes are thought to resemble the characteristics of early-passage MSCs, while larger cell sizes may be indicative of senescence [32,33]. The cell size distribution of MSCs within self-assembled constructs showed somewhat greater increases at 14 days, implying that senescence-associated changes might have started occurring at this time (Fig. 3o). In contrast, MSCs grown in non-self-assembled microniches showed evidence of senescence through SA-β-Gal staining at as early as 3–7 days (Fig. 3p). These results collectively indicate that the optimal maintenance of stemness and suppression of senescence in MSCs occurs while cultured in self-assembled constructs at 7 days.

The paracrine function of MSCs in self-assembled constructs was assessed over 14 days by comparing their cytokine profile between time points (cytokine array blots shown in Fig. S3, quantitative expression of all cytokines presented in Table S5). There were 8 cytokines that exhibited significantly different staining intensity among the different time points, all of which increased with time (Fig. 3q). The paracrine function of MSCs within self-assembled constructs therefore appears to increase with time and is independent of the observed changes in cell stemness and senescence.

3.3. Mechanism for self-assembly of MSC-laden microniches into functional constructs

We previously demonstrated that MSCs growing in microniches had ECM accumulation and functional enhancement [19]. In this study, we hypothesised that ECM accumulation contributed to the mechanism of microniche self-assembly by enhancing cell-cell or cell-ECM interactions (MOVIE S2).

The protein profile of self-assembled constructs was analysed through quantitative proteomic characterisation at 0, 3, 7 and 14 days of culture (Fig. 4a). A total of 199 proteins were identified with higher expression and 1077 proteins with lower expression, which were drawn as a heat map (Fig. 4b). Numbers of proteins with higher expression showed significant fold change over 14 days, such as COL4A2 and SOD2, and their expression levels were plotted as a line chart (Fig. 4c). Most of these trends were further confirmed by Western blot (Fig. 4d). The highly expressed proteins in MSCs during construct self-assembly were mainly ECM-related proteins, such as collagens, fibronectin and LOXL2, which can provide binding sites to matrix components or cell surface receptors and help facilitate cell-matrix interactions to form a complex 3D network [34].

In protein-protein interaction (PPI) analysis, the 199 differentially upregulated proteins were classified into four clusters based on their functions: ECM organisation and receptor, collagen binding, glycolytic metabolism, and mitochondrial electron transport (Fig. 4e). The molecular activities of these proteins, such as catalytic activity, binding and molecular function regulator, were sum-

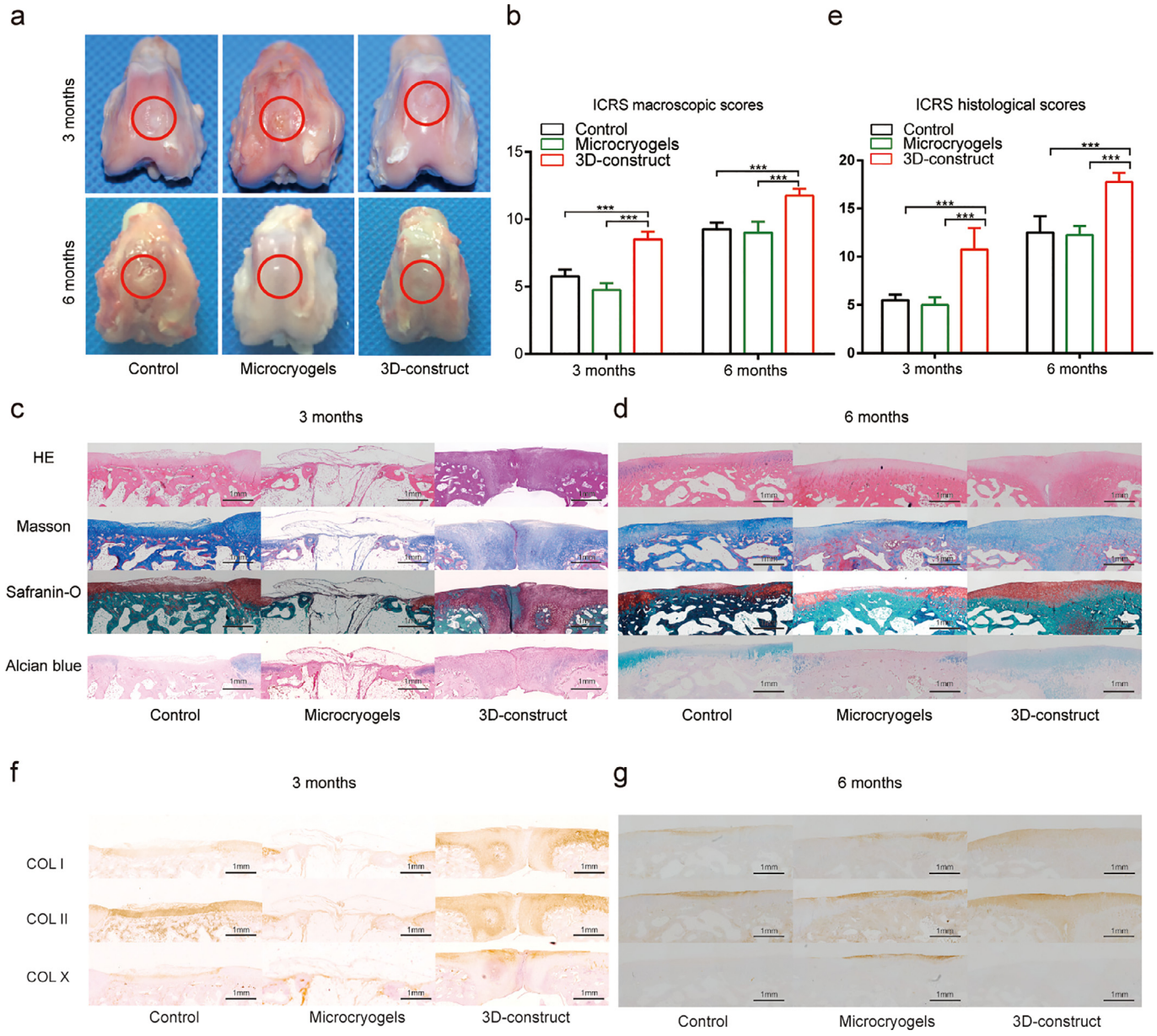


Fig. 5. Using self-assembled constructs for *in vivo* cartilage repair. (A) Improved macroscopic repair was observed in the 3D-construct group compared to other groups at 3 and 6 months. (B) ICRS macroscopic assessment scores were the highest in the 3D-construct group compared to other groups at both 3 and 6 months ($p < 0.01$, $n = 4$). (C,D) H&E, Masson's trichrome, Safranin O and Alcian blue staining of repaired defects, showing that the 3D-construct group had the best overall repair compared to microcryogels and control groupsat both 3 and 6 months. (E) ICRS histological assessment scores were the highest in the 3D-construct group compared to other groups at both 3 and 6 months ($p < 0.01$, $n = 4$). (F, G) Immunohistochemical staining for collagen type II, I and X at 3 and 6 months after surgery showed that the 3D-construct group had the highest proportion of hyaline cartilage-like tissue compared to other groups.

marised in a pie chart using the PANTHER bioinformatics platform (Fig. 4f). Enrichment analysis of gene ontology (GO) showed that upregulated proteins were mostly related to ECM components, while signal pathways were mainly related to ECM-receptor interactions (Fig. 4g). Collectively, these findings suggest that construct self-assembly is induced by the accumulation of ECM components in individual microniches during culture, which strengthen cell-ECM interactions that connect adjacent microniches to form a functional construct.

3.4. *Using self-assembled constructs for* in vivo *cartilage repair*

3.4.1. *Clinical observations following construct implantation*

A rabbit femoral trochlear cartilage defect model was used for construct implantation (Fig. S4). The self-assembled constructs were easy to handle and manipulate during implantation without fretting or disintegration, and were seen to fill the defects well immediately after implantation. All animals recovered well without signs of distress or limping for the duration of the study, and no post-operative complications were observed over the 6 months.

3.4.2. *Macroscopic assessment of cartilage defect repair*

At 3 months after surgery, macroscopic observations showed that the cartilage defects repaired using the 3D-construct group had a flat surface and were almost completely filled with regenerated tissue (Fig. 5a). The new tissue had a similar appearance to the surrounding normal cartilage, although an indistinct border was present. In contrast, defects repaired using the microcryogels and control groups were only partly filled with repair tissue and had an irregular surface. The repair tissue had a soft texture

and distinct defect borders were evident. At 6 months, the defects were almost completely filled with repair tissue in all groups. Close examination showed that the 3D-construct group had better integration with the surrounding normal cartilage and a more regular defect surface than the other two groups. The ICRS macroscopic assessment scores for the 3D-construct group were significantly higher than the other two groups at both 3 and 6 months (Fig. 5b).

3.4.3. Histological evaluation of cartilage defect repair

At 3 months after surgery, the defects were filled with hyaline-like cartilage in the 3D-construct group as shown by staining with H&E for tissue composition and arrangement, Masson's trichrome for collagen arrangement, Safranin O for glycosaminoglycans, and Alcian blue for chondrocytes (Fig. 5c). In contrast, the defects in the microcryogels and control groups were mostly filled with fibrous tissue. At 6 months, defects in all groups were almost completely filled with newly formed tissues (Fig. 5d). Defects in the 3D-construct group were repaired with hyaline-like cartilage, with similar histological features as surrounding normal cartilage as shown by intense Safranin O and Alcian blue staining, indicating superior cartilage repair. In contrast, the microcryogels and control groups were filled with a mixture of fibrous and cartilage-like tissue. The ICRS histological assessment scores for repair tissue in the 3D-construct group were significantly higher than the other two groups at both 3 and 6 months (Fig. 5e).

3.4.4. Immunohistochemical analysis of cartilage defect repair

At 3 months after surgery, immunohistochemical staining showed markedly positive collagen type I and II staining in the 3D-construct group compared to the other two groups (Fig. 5f), suggesting that the defect was filled with both fibrous and hyaline-like cartilage tissues. The accumulation of collagen type II with concomitant increase in collagen types I and X might indicate an enhancement of chondrogenesis with some induction of terminal differentiation, as well as endochondral ossification within the subchondral bone. The self-assembled constructs facilitated faster repair of the cartilage defect compared to the microcryogels and control groups. At 6 months, the 3D-construct group showed the highest amount of collagen type II staining on the surface of the repair tissue, indicating significant formation of hyaline-like cartilage (Fig. 5g). A small amount of collagen type I staining was evident in all groups, indicating the presence of some fibrous cartilage-like tissue. Collagen type X staining was only evident in the microcryogels group, which might indicate progression towards degradation or calcification of the cartilage-like tissue in the superficial layer. Furthermore, anti-human Ki67 staining indicated that cartilage repair was likely facilitated by the paracrine function of implanted MSCs, which might have induced homing of autologous cells or immunomodulation (Fig. S5).

4. Discussion

In this study, we have developed a method of forming 3D macroscopic tissue constructs through self-assembly. For the first time, cell-laden porous gelatin microcryogels are induced to self-assemble during culture in 3D-printed frames to form functional tissue constructs with a predefined shape. Although some other bio-scaffolds have been reported that may prevent MSC senescence and promote cell function, these scaffolds were mostly artificially synthesised rather than self-assembled through a natural process. The microniches used for self-assembly in this study are essentially microscopic cellular units that are maintained in a relatively 'native' microenvironment, and the process of self-assembly allows the microniches to connect with each other and form a macroscopic cellular construct.

The mechanism of construct formation was likely related to ECM accumulation in the microniches, which enabled connections with cells and ECM in adjacent microniches resulting in self-assembly. This provided a 3D microenvironment that better facilitated the maintenance of MSC function [35]. Proteomic and bioinformatic analyses showed that when MSCs were growing within self-assembled constructs compared to in individual microniches or monolayer, they had higher expression of ECM-related proteins over time. For instance, LOXL2 was one of the highly expressed proteins in self-assembled constructs, which catalyses the first step of covalent cross-linking for collagens and elastin in the ECM, a process that confers ECM stiffness and mechanical properties [36]. Fibronectin (FN1), another highly expressed protein, is known as a master organiser of several ECM fibre systems and is deposited early in the process of ECM formation. It is essential for the formation of fibrillin-1 (FBN-1) containing microfibrils, as well as collagen types I and III [37]. During ECM accumulation, fibronectin can be retained within cellularised scaffolds and promote elastin deposition, matrix elasticity and mechanical strength [38]. Fibrillins (such as fibrillin-1 that was highly expressed) constitute the major backbone of multifunctional microfibrils, and their assembly is achieved by binding with fibronectin through the collagen/gelatin-binding region [39]. In addition, relatively stable TIMP3 protein expression during self-assembly over 14 days indicated a balance between ECM deposition and degradation. These findings suggested that construct self-assembly was initiated by spontaneous aggregation of microniches following ECM accumulation within the microniches, which promoted cell-cell and cell-ECM interactions that strengthened the cohesiveness of the assembling microniches. This induced construct self-assembly through the formation of a complex ECM network that is unachievable in individual microniches, providing a more 'native' microenvironment for the MSCs to perform their functions [40].The increasing protein expression of SOD2 with culture duration also indicated stronger antioxidant protection and modulation of apoptosis, which might have resulted in better preservation of MSC survival and quality, as well as resistance of external and internal stresses [41]. While these protein analyses gave significant insights into the mechanisms of construct self-assembly, it was beyond the scope of this study to block the ECM proteins displaying the highest changes in expression to investigate whether this would inhibit the microniches from undergoing self-assembly. This will be addressed in our future studies.

The ECM is an intricate and dynamic bio-environment with precisely regulated mechanical and biochemical properties [42]. In tissue regeneration, the ECM is involved in regulating cell adhesion, proliferation, responses to growth factors, differentiation, and ultimately the functional characteristics of the mature tissue. With rapid advances in regenerative medicine, scaffolds that can provide regulation of MSC behaviour through the ECM have attracted increasing attention. MSCs regulate their fate by binding to the extracellular environment, where they may be exposed to various chemicals, and physical and mechanical signals [43]. The ECM therefore has a profound influence on MSC fate, notably through its geometry/topography and mechanical properties, as well as through the transmission of mechanical or other biophysical factors to the MSCs [44]. These influences are particularly important in 3D functional tissue constructs that better mimic native cell-ECM interactions, and likely have contributed to maintaining the beneficial properties of MSCs in the self-assembled constructs in this study.

In this study, functional analysis of the self-assembled constructs showed that MSCs could better maintain stemness, suppress senescence and promote paracrine function compared to cells grown in non-self-assembled microniches. This might help address a primary challenge in current cell-based tissue engineer-

ing approaches. The efficacy of current cell therapy for tissue regeneration is not satisfactory due to poor retention, survival and function of the transplanted cells. For instance, for the umbilical cord-derived MSCs which were used as the model cells in this study, their quality has been reported to decline with culture duration and long-term expansion [45]. The loss of cell stemness with aging is accompanied by decreased cell proliferation, increase in cell size, and expression of β-Gal and Annexin-V as markers of senescence [46,47]. By culturing MSCs on native or biomimetic ECM, the cells can better retain their phenotype, proliferation capacity and differentiation potential for prolonged culture durations [48], and may in part combat some of the effects of cell senescence. In this study, culture within self-assembled constructs significantly improved stemness in MSCs and delayed their senescence, suggesting that these constructs were more effective at providing the cells with a native microenvironmental 'niche'. We further confirmed that there was an optimal time point at which the cells exhibited maximum functionality within the constructs, which was at 7 days following the initial induction of self-assembly. For tissue regeneration applications, this can also be considered as the optimal pre-culture time period to form the construct prior to implantation.

The ability of MSCs to produce paracrine effectors is an important mechanism in many processes associated with tissue regeneration [49,50]. In this study, the macroscopic and microscopic stiffness of the self-assembled constructs, as determined through mechanical testing, were observed to increase with time. This is likely due to increasing ECM deposition, organisation and maturation within the construct during self-assembly, which would enhance its mechanical properties. Changes in mechanical cues within the microenvironment, arising from the ECM [51,52] or other substrate [53,54] have been shown to directly influence the paracrine activity of MSCs. The enhanced paracrine function of MSCs during construct self-assembly may be at least be partly related to the increase in construct mechanical properties. Furthermore, ECM accumulation during self-assembly can also contribute to upregulating MSC paracrine activities relating to anti-inflammatory effects and cell recruitment to injury sites [55,56].

We further tested the ability of the self-assembled constructs to be used as functional scaffolds for inducing tissue repair, using a cartilage defect model as an example. The cartilage model was selected since articular cartilage is very difficult to repair once damaged due to its avascularity, low cellularity and low tissue turnover [57]. Articular cartilage defects are usually irregular in nature and repair through tissue engineered approaches require seamless integration between the implant and surrounding native cartilage. Furthermore, cartilage defects with clinically relevant sizes require macroscopically-sized constructs [58], which are preferably metabolically active with viable cells throughout to initiate repair and tissue integration following implantation. These requirements are very difficult to achieve using traditional fixed-size bulk scaffolds, which often cannot fit irregular defects perfectly, and are prone to developing cell necrosis in the centre region due to limited nutrient transport. The self-assembled constructs in this study provided a solution to such problems. 3D printing was used to develop a precisely shaped frame and grid base that could maintain adequate spacing between microniches for optimal nutrient transport, as well as avoid microniche leakage. The size and shape of self-assembled constructs could be well controlled by modifying the dimensions and shape of the 3D-printed frame used to guide construct formation. Being built from microscopic hydrogels, the self-assembled constructs were soft and resilient, which could be easily trimmed and manipulated to suit the defect if required. Furthermore, the entire construct would remain functional and viable following implantation since it consists of microscopic cell-laden units. The microcyogels which form the basis of these cellular units are highly porous and do not require physical or chemical cross-linking during cell seeding, which greatly preserve cell viability and function when the units are undergoing self-assembly. In a rabbit articular cartilage defect model, the self-assembled constructs showed superior ability to induce defect repair through the formation of hyaline-like cartilage, which was not observed in defects filled with microcryogels alone or the control group. These findings suggest that the self-assembled constructs can be used as alternative tissue engineered implants to promote *in vivo* repair of certain challenging tissue defects. Future studies will evaluate the potential of inducing construct self-assembly *in situ*, which should allow better defect filling as the microniches would assume the shape of the defect once implanted. The efficacy of these constructs compared to bulk scaffolds or hydrogels constructed using similar base materials will also be investigated. Since MSCs are sensitive to the physical, biochemical and mechanical microenvironment, pre-conditioning of cells before and after microcryogel self-assembly to mimic the native tissue niche may produce constructs that are useful for other tissue types, such as tendon and skeletal muscle [59]. Furthermore, the self-assembled constructs have potential to be developed as a 'bioink' for bioprinting strategies to create complex 3D functional tissues such as skin, bone and some artificial organs [60].

5. Conclusion

In this study, we developed 3D functional tissue constructs by inducing self-assembly of microniches consisting of MSC-laden microcryogels. The self-assembled constructs showed superior ability to maintain phenotypic characteristics and stemness in MSCs, while suppressing their senescence and enhancing their paracrine functions. The mechanism of self-assembly was shown to be related to ECM accumulation that strengthened cell-ECM interactions within the construct. The self-assembled constructs successfully repaired articular cartilage defects *in vivo* without the need to introduce additional factors. This strategy for developing 3D macroscopic tissue constructs allows the optimisation of stem cell functions and construction of biomimetic tissue organoids, with the potential to be applied for a wide variety of tissues and tissue engineering applications.

Declaration of Competing Interest

The authors declare that they have no conflict of interest.

Acknowledgments

We gratefully acknowledge Dr Yaozu Wu and Dr Shumeng Jiang for their assistance in preparing the gelatin scaffolds, as well as Beijing CytoNiche Biotechnology Ltd for providing technical support. We also thank Dr Jialu Ma, Dr Huizhen Cao and Dr Yue Sun from the Center of Biomedical Analysis at Tsinghua University for technical assistance.

Funding

This study was supported by grants from the National Natural Science Foundation of China (No. 81973606, 81873316, 81673994), Peking University People's Hospital Scientific Research Development Funds (No. RDY 2019-11, RS 2019-03), Beijing Science and Technology Major Projects (No. Z181100001818008), and the Australian National Health and Medical Research Council (APP1120249).

Supplementary materials

Supplementary material associated with this article can be found, in the online version, at doi:10.1016/j.actbio.2020.07.058.

References

[1] F. Xing, L. Li, C. Zhou, C. Long, L. Wu, H. Lei, Q. Kong, Y. Fan, Z. Xiang, X. Zhang, Regulation and directing stem cell fate by tissue engineering functional microenvironments: scaffold physical and chemical cues, Stem Cells Int. 2019 (2019) 2180925.

[2] K.H. Vining, D.J. Mooney, Mechanical forces direct stem cell behaviour in development and regeneration, Nat. Rev. Mol. Cell Biol. 18 (12) (2017) 728–742.

[3] C. Zhang, B. Xie, Y. Zou, D. Zhu, L. Lei, D. Zhao, H. Nie, Zero-dimensional, one-dimensional, two-dimensional and three-dimensional biomaterials for cell fate regulation, Adv. Drug Deliv. Rev. 132 (2018) 33–56.

[4] Y. Ma, M. Lin, G. Huang, Y. Li, S. Wang, G. Bai, T.J. Lu, F. Xu, 3D spatiotemporal mechanical microenvironment: a hydrogel-based platform for guiding stem cell fate, Adv. Mater. Weinheim 30 (49) (2018) e1705911.

[5] C.M. Madl, S.C. Heilshorn, Engineering hydrogel microenvironments to recapitulate the stem cell niche, Annu. Rev. Biomed. Eng. 20 (2018) 21–47.

[6] A.I. Marusina, A.A. Merleev, J.I. Luna, L. Olney, N.E. Haigh, D. Yoon, C. Guo, E.M. Ovadia, M. Shimoda, G. Luxardi, S. Boddu, N.N. Lal, Y. Takada, K.S. Lam, R. Liu, R.R. Isseroff, S. Le, J.A. Nolta, A.M. Kloxin, E. Maverakis, Tunable hydrogels for mesenchymal stem cell delivery: Integrin-induced transcriptome alterations and hydrogel optimization for human wound healing, Stem Cells 38 (2) (2020) 231–245.

[7] K.H. Hong, Y.M. Kim, S.C. Song, Fine-tunable and injectable 3D hydrogel for on-demand stem cell niche, Adv. Sci. (Weinh) 6 (17) (2019) 1900597.

[8] P.K. Mishra, C.M. Yoo, E. Hong, H.W. Rhee, Photo-crosslinking: an emerging chemical tool for investigating molecular networks in live cells, Chembiochem 21 (7) (2020) 924–932.

[9] R. Parhi, Cross-linked hydrogel for pharmaceutical applications: a review, Adv. Pharm Bull. 7 (4) (2017) 515–530.

[10] Z. Naghizadeh, A. Karkhaneh, A. Khojasteh, Self-crosslinking effect of chitosan and gelatin on alginate based hydrogels: Injectable in situ forming scaffolds, Mater Sci Eng. C Mater Biol. Appl. 89 (2018) 256–264.

[11] K. Adamiak, A. Sionkowska, Current methods of collagen cross-linking: Review, Int. J. Biol. Macromol. 161 (2020) 550–560.

[12] X. Wang, S. Liu, Q. Zhao, N. Li, H. Zhang, X. Zhang, X. Lei, H. Zhao, Z. Deng, J. Qiao, Y. Cao, L. Ning, S. Liu, E. Duan, Three-dimensional hydrogel scaffolds facilitate in vitro self-renewal of human skin-derived precursors, Acta Biomater 10 (7) (2014) 3177–3187.

[13] S. Darouie, S. Ansari Majd, F. Rahimi, E. Hashemi, M. Kabirsalmani, A. Dolatshahi-Pirouz, A. Arpanaei, The fate of mesenchymal stem cells is greatly influenced by the surface chemistry of silica nanoparticles in 3D hydrogel-based culture systems, Mater Sci. Eng. C Mater Biol. Appl. 106 (2020) 110259.

[14] B.P. Mahadik, N.A. Bharadwaj, R.H. Ewoldt, B.A. Harley, Regulating dynamic signaling between hematopoietic stem cells and niche cells via a hydrogel matrix, Biomaterials 125 (2017) 54–64.

[15] Y. Chen, J. Sui, Q. Wang, Y. Yin, J. Liu, Q. Wang, X. Han, Y. Sun, Y. Fan, X. Zhang, Injectable self-crosslinking HA-SH/Col I blend hydrogels for in vitro construction of engineered cartilage, Carbohydr Polym 190 (2018) 57–66.

[16] R. Resmi, J. Parvathy, A. John, R. Joseph, Injectable self-crosslinking hydrogels for meniscal repair: A study with oxidized alginate and gelatin, Carbohydr Polym 234 (2020) 115902.

[17] D. Ghosh Dastidar, S. Saha, M. Chowdhury, Porous microspheres: Synthesis, characterisation and applications in pharmaceutical & medical fields, Int. J. Pharm. 548 (1) (2018) 34–48.

[18] W. Liu, Y. Li, Y. Zeng, X. Zhang, J. Wang, L. Xie, X. Li, Y. Du, Microcryogels as injectable 3-D cellular microniches for site-directed and augmented cell delivery, Acta Biomater 10 (5) (2014) 1864–1875.

[19] Y. Li, W. Liu, F. Liu, Y. Zeng, S. Zuo, S. Feng, C. Qi, B. Wang, X. Yan, A. Khademhosseini, J. Bai, Y. Du, Primed 3D injectable microniches enabling low-dosage cell therapy for critical limb ischemia, Proc. Natl. Acad. Sci. U.S.A. 111 (37) (2014) 13511–13516.

[20] Y. Zeng, C. Chen, W. Liu, Q. Fu, Z. Han, Y. Li, S. Feng, X. Li, C. Qi, J. Wu, D. Wang, C. Corbett, B.P. Chan, D. Ruan, Y. Du, Injectable microcryogels reinforced alginate encapsulation of mesenchymal stromal cells for leak-proof delivery and alleviation of canine disc degeneration, Biomaterials 59 (2015) 53–65.

[21] C. Qi, Y. Li, P. Badger, H. Yu, Z. You, X. Yan, W. Liu, Y. Shi, T. Xia, J. Dong, C. Huang, Y. Du, Pathology-targeted cell delivery via injectable micro-scaffold capsule mediated by endogenous TGase, Biomaterials 126 (2017) 1–9.

[22] J. Wang, F. Chen, L. Liu, C. Qi, B. Wang, X. Yan, C. Huang, W. Hou, M.Q. Zhang, Y. Chen, Y. Du, Engineering EMT using 3D micro-scaffold to promote hepatic functions for drug hepatotoxicity evaluation, Biomaterials 91 (2016) 11–22.

[23] Y. Zeng, L. Zhu, Q. Han, W. Liu, X. Mao, Y. Li, N. Yu, S. Feng, Q. Fu, X. Wang, Y. Du, R.C. Zhao, Preformed gelatin microcryogels as injectable cell carriers for enhanced skin wound healing, Acta Biomater 25 (2015) 291–303.

[24] S. Jiang, C. Lyu, P. Zhao, W. Li, W. Kong, C. Huang, G.M. Genin, Y. Du, Cryoprotectant enables structural control of porous scaffolds for exploration of cellular mechano-responsiveness in 3D, Nat Commun. 10 (1) (2019) 3491.

[25] X. Fan, L. Zhu, K. Wang, B. Wang, Y. Wu, W. Xie, C. Huang, B.P. Chan, Y. Du, Stiffness-Controlled Thermoresponsive Hydrogels for Cell Harvesting with Sustained Mechanical Memory, Adv Healthc. Mater 6 (5) (2017).

[26] F. Li, V.X. Truong, P. Fisch, C. Levinson, V. Glattauer, M. Zenobi-Wong, H. Thissen, J.S. Forsythe, J.E. Frith, Cartilage tissue formation through assembly of microgels containing mesenchymal stem cells, Acta Biomater 77 (2018) 48–62.

[27] F. Li, C. Levinson, V.X. Truong, L.A. Laurent-Applegate, K. Maniura-Weber, H. Thissen, J.S. Forsythe, M. Zenobi-Wong, J.E. Frith, Microencapsulation improves chondrogenesis in vitro and cartilaginous matrix stability in vivo compared to bulk encapsulation, Biomater Sci. 8 (6) (2020) 1711–1725.

[28] M.B. Murphy, K. Moncivais, A.I. Caplan, Mesenchymal stem cells: environmentally responsive therapeutics for regenerative medicine, Exp. Mol. Med. 45 (2013) e54.

[29] Y. Hu, H. Wang, Q. Wang, H. Deng, Overexpression of CD38 decreases cellular NAD levels and alters the expression of proteins involved in energy metabolism and antioxidant defense, J. Proteome Res 13 (2) (2014) 786–795.

[30] Y. Li, Y. Gong, X. Wu, F. Wang, Y. Xie, Z. Zhu, Y. Su, J. Wang, C. Zhang, J. He, H. Deng, S. Wang, Quantitative proteomic analysis of deciduous molars during cap to bell transition in miniature pig, J. Proteomics 172 (2018) 57–67.

[31] P. Mainil-Varlet, B. Van Damme, D. Nesic, G. Knutsen, R. Kandel, S. Roberts, A new histology scoring system for the assessment of the quality of human cartilage repair: ICRS II, Am. J. Sports Med. 38 (5) (2010) 880–890.

[32] D.C. Colter, R. Class, C.M. DiGirolamo, D.J. Prockop, Rapid expansion of recycling stem cells in cultures of plastic-adherent cells from human bone marrow, Proc. Natl. Acad. Sci. U.S.A. 97 (7) (2000) 3213–3218.

[33] C.P. Ng, A.R. Sharif, D.E. Heath, J.W. Chow, C.B. Zhang, M.B. Chan-Park, P.T. Hammond, J.K. Chan, L.G. Griffith, Enhanced ex vivo expansion of adult mesenchymal stem cells by fetal mesenchymal stem cell ECM, Biomaterials 35 (13) (2014) 4046–4057.

[34] A.D. Theocharis, S.S. Skandalis, C. Gialeli, N.K. Karamanos, Extracellular matrix structure, Adv. Drug Deliv. Rev. 97 (2016) 4–27.

[35] T. Wang, S.S. Nanda, G.C. Papaefthymiou, D.K. Yi, Mechanophysical cues in extracellular matrix regulation of cell behavior, Chembiochem (2019).

[36] S.D. Vallet, S. Ricard-Blum, Lysyl oxidases: from enzyme activity to extracellular matrix cross-links, Essays Biochem. 63 (3) (2019) 349–364.

[37] J. Sottile, D.C. Hocking, Fibronectin polymerization regulates the composition and stability of extracellular matrix fibrils and cell-matrix adhesions, Mol. Biol. Cell 13 (10) (2002) 3546–3559.

[38] D. Pezzoli, J. Di Paolo, H. Kumra, G. Fois, G. Candiani, D.P. Reinhardt, D. Mantovani, Fibronectin promotes elastin deposition, elasticity and mechanical strength in cellularised collagen-based scaffolds, Biomaterials 180 (2018) 130–142.

[39] L. Sabatier, D. Chen, C. Fagotto-Kaufmann, D. Hubmacher, M.D. McKee, D.S. Annis, D.F. Mosher, D.P. Reinhardt, Fibrillin assembly requires fibronectin, Mol. Biol. Cell 20 (3) (2009) 846–858.

[40] K.E. Scott, K. Rychel, S. Ranamukhaarachchi, P. Rangamani, S.I. Fraley, Emerging themes and unifying concepts underlying cell behavior regulation by the pericellular space, Acta Biomater 96 (2019) 81–98.

[41] S. Magalhães-Novais, J.C. Bermejo-Millo, R. Loureiro, K.A. Mesquita, M.R. Domingues, E. Maciel, T. Melo, I. Baldeiras, J.R. Erickson, J. Holy, Y. Potes, A. Coto-Montes, P.J. Oliveira, I. Vega-Naredo, Cell quality control mechanisms maintain stemness and differentiation potential of P19 embryonic carcinoma cells, Autophagy 16 (2) (2020) 313–333.

[42] X. Lin, S. Patil, Y.G. Gao, A. Qian, The bone extracellular matrix in bone formation and regeneration, Front Pharmacol. 11 (2020) 757.

[43] W.P. Daley, S.B. Peters, M. Larsen, Extracellular matrix dynamics in development and regenerative medicine, J. Cell. Sci. 121 (Pt 3) (2008) 255–264.

[44] M. Tatullo, M. Marrelli, G. Falisi, C. Rastelli, F. Palmieri, M. Gargari, B. Zavan, F. Paduano, V. Benagiano, Mechanical influence of tissue culture plates and extracellular matrix on mesenchymal stem cell behavior: A topical review, Int. J. Immunopathol. Pharmacol. 29 (1) (2016) 3–8.

[45] J. Kim, J.W. Kang, J.H. Park, Y. Choi, K.S. Choi, K.D. Park, D.H. Baek, S.K. Seong, H.K. Min, H.S. Kim, Biological characterization of long-term cultured human mesenchymal stem cells, Arch. Pharm. Res. 32 (1) (2009) 117–126.

[46] R.X. Wu, C.S. Bi, Y. Yu, L.L. Zhang, F.M. Chen, Age-related decline in the matrix contents and functional properties of human periodontal ligament stem cell sheets, Acta Biomater 22 (2015) 70–82.

[47] T.J. Block, M. Marinkovic, O.N. Tran, A.O. Gonzalez, A. Marshall, D.D. Dean, X.D. Chen, Restoring the quantity and quality of elderly human mesenchymal stem cells for autologous cell-based therapies, Stem Cell Res Ther. 8 (1) (2017) 239.

[48] A. Shakouri-Motlagh, A.J. O'Connor, S.P. Brennecke, B. Kalionis, D.E. Heath, Native and solubilized decellularized extracellular matrix: A critical assessment of their potential for improving the expansion of mesenchymal stem cells, Acta Biomater 55 (2017) 1–12.

[49] M. Mastri, H. Lin, T. Lee, Enhancing the efficacy of mesenchymal stem cell therapy, World J. Stem Cells 6 (2) (2014) 82–93.

[50] L. Yin, Z. Yang, Y. Wu, V. Denslin, C.C. Yu, C.A. Tee, C.T. Lim, J. Han, E.H. Lee, Label-free separation of mesenchymal stem cell subpopulations with distinct differentiation potencies and paracrine effects, Biomaterials 240 (2020) 119881.

[51] K.E. Sullivan, K.P. Quinn, K.M. Tang, I. Georgakoudi, L.D. Black 3rd, Extracellular matrix remodeling following myocardial infarction influences the therapeutic potential of mesenchymal stem cells, Stem Cell Res. Ther. 5 (1) (2014) 14.

[52] S. Jose, M.L. Hughbanks, B.Y. Binder, G.C. Ingavle, J.K. Leach, Enhanced trophic factor secretion by mesenchymal stem/stromal cells with Glycine-Histidine-Lysine (GHK)-modified alginate hydrogels, Acta Biomater 10 (5) (2014) 1955–1964.
[53] F.P. Seib, M. Prewitz, C. Werner, M. Bornhäuser, Matrix elasticity regulates the secretory profile of human bone marrow-derived multipotent mesenchymal stromal cells (MSCs), Biochem. Biophys. Res. Commun. 389 (4) (2009) 663–667.
[54] H. Yang, K.T. Nguyen, D.T. Leong, N.S. Tan, C.Y. Tay, Soft material approach to induce oxidative stress in mesenchymal stem cells for functional tissue repair, ACS Appl Mater Interfaces 8 (40) (2016) 26591–26599.
[55] J.M. Santos, S.P. Camões, E. Filipe, M. Cipriano, R.N. Barcia, M. Filipe, M. Teixeira, S. Simões, M. Gaspar, D. Mosqueira, D.S. Nascimento, P. Pinto-do-Ó, P. Cruz, H. Cruz, M. Castro, J.P. Miranda, Three-dimensional spheroid cell culture of umbilical cord tissue-derived mesenchymal stromal cells leads to enhanced paracrine induction of wound healing, Stem Cell Res. Ther. 6 (2015) 90.
[56] E.J. Lee, S.J. Park, S.K. Kang, G.H. Kim, H.J. Kang, S.W. Lee, H.B. Jeon, H.S. Kim, Spherical bullet formation via E-cadherin promotes therapeutic potency of mesenchymal stem cells derived from human umbilical cord blood for myocardial infarction, Mol. Ther 20 (7) (2012) 1424–1433.
[57] T.A. Ahmed, M.T. Hincke, Strategies for articular cartilage lesion repair and functional restoration, Tissue Eng. Part B Rev. 16 (3) (2010) 305–329.
[58] J.L. Jiao, D.L. Kaplan, H. Zreiqat, Scaffold-based regeneration of skeletal tissues to meet clinical challenges, J. Mater Chem. B 2 (2014).
[59] M. Beldjilali-Labro, A. Garcia Garcia, F. Farhat, F. Bedoui, J.F. Grosset, M. Dufresne, C. Legallais, Biomaterials in Tendon and Skeletal Muscle Tissue Engineering: Current Trends and Challenges, Materials (Basel) 11 (7) (2018).
[60] C. Mandrycky, Z. Wang, K. Kim, D.H. Kim, 3D bioprinting for engineering complex tissues, Biotechnol. Adv. 34 (4) (2016) 422–434.